



Mapping gaseous amines, ammonia, and their particulate counterparts in marine atmospheres of China's marginal seas: Part 1 - Differentiating marine emission from continental transport

Dihui Chen¹, Yanjie Shen¹, Juntao Wang¹, Yang Gao^{1,2}, Huiwang Gao^{1,2}, Xiaohong Yao^{1,2*}

5 ¹Key Laboratory of Marine Environment and Ecology, and Frontiers Science Center for Deep Ocean Multispheres and Earth System, Ministry of Education, Ocean University of China, Qingdao 266100, China

²Laboratory for Marine Ecology and Environmental Science, Qingdao National Laboratory for Marine Science and Technology, Qingdao 266237, China

* *correspondence to:* Xiaohong Yao (xhyao@ouc.edu.cn)

10 **Abstract.** To study sea-derived gaseous amines, ammonia, and primary particulate aminium ions in the marine atmospheres of China's marginal seas, an onboard URG-9000D Ambient Ion Monitor-Ion chromatography (AIM-IC, Thermo Fisher) was set up on the front deck of the R/V Dongfanghong 3 to semi-continuously measure the spatiotemporal variations in the concentrations of atmospheric trimethylamine (TMA_{gas}), dimethylamine (DMA_{gas}), and ammonia (NH_{3gas}) along with their particulate matter (PM_{2.5}) counterparts. In this study, we differentiated marine emissions of the gas species originating from

15 continental transport using data obtained from December 9 to 22, 2019 during the cruise over the Yellow and Bohai Seas, facilitated by additional measurements collected at a coastal site near the Yellow Sea during summer 2019. The data obtained during the cruise and the coastal site demonstrated that the observed TMA_{gas} and protonated trimethylamine (TMAH⁺) in PM_{2.5} over the Yellow and Bohai Seas overwhelmingly originated from marine sources. During the cruise, there was no significant correlation (P>0.05) between the simultaneously measured TMAH⁺ and TMA_{gas} concentrations.

20 Additionally, the concentrations of TMAH⁺ in the marine atmosphere varied around 0.28±0.18 μg m⁻³ (average ± standard deviation), with several episodic hourly average values exceeding 1 μg m⁻³, which were approximately one order of magnitude larger than those of TMA_{gas} (approximately 0.031±0.009 μg m⁻³). Moreover, there was a significant negative correlation (P<0.01) between the concentrations of TMAH⁺ and NH₄⁺ in PM_{2.5} during the cruise. Therefore, the observed TMAH⁺ in PM_{2.5} was overwhelmingly derived from primary sea-spray aerosols. Using the TMA_{gas} and TMAH⁺ in PM_{2.5} as

25 tracers for sea-derived basic gases and sea-spray particulate aminium ions, the values of non-sea-derived DMA_{gas} and NH_{3gas},



as well as non-sea-spray particulate DMAH⁺ in PM_{2.5}, were estimated, and the estimated average values of each species contributed to 16%, 34%, and 65% of the observed average concentrations, respectively. Uncertainties remained in the estimations as TMAH⁺ may decompose into smaller molecules in seawater to varying extents. The non-sea-derived gases and non-sea-spray particulate DMAH⁺ likely originated from long-range transport from the upwind continents, according to the recorded offshore winds and increased concentrations of SO₄²⁻ and NH₄⁺ in PM_{2.5}. The lack of a detectable increase in the particulate DMAH⁺, NH₄⁺, and SO₄²⁻ concentrations in several SO₂ plumes did not support the secondary formation of particulate DMAH⁺ in the marine atmosphere.

Keywords: Marine atmospheric NH₃, trimethylamine, dimethylamine, particulate aminium, sea-spray aerosol

Introduction

Gaseous amines and their particulate counterparts are important reduced nitrogen compounds in the marine atmosphere (Facchini et al., 2008; Müller et al., 2009; Hu et al., 2015; Hu et al., 2018; van Pinxteren et al., 2015; van Pinxteren et al., 2019; Yu et al., 2016; Xie et al., 2018; Zhou et al., 2019) and are primarily derived from the degradation of glycine betaine (GBT), trimethylamine N-oxide (TMAO), and choline (Burg and Ferraris, 2008; Lidbury et al., 2015a; Lidbury et al., 2015b; Jameson et al., 2016; Taubert et al., 2017). GBT, TMAO, and choline are critical for maintaining osmotic pressure in marine organisms. When released into the environment, they can be degraded by bacteria to trimethylamine (TMA) and then dimethylamine (DMA) or methylamines (MA) (Lidbury et al., 2015a; Lidbury et al., 2015b). Gaseous DMA, TMA, and MA may play an important role in the formation of secondary particles in the atmosphere by nucleation (Almeida et al., 2013; Chen et al., 2016; Yao et al., 2018; Zhu et al., 2019). However, measuring gaseous amines in real-time simultaneously to their particulate counterparts in the marine atmosphere over the ocean remains challenging, although this is not the case in the continental atmosphere (VandenBoer et al., 2011). The lack of direct measurements restricts the determination of their sources and the relationship between the reduced nitrogen compounds and acid-base neutralization reactions in the marine atmosphere.

Reduced nitrogen compounds in the ocean can finally decompose into ammonium ions (NH₄⁺) and other smaller molecules.



NH₄⁺ in surface seawater releases to the marine atmosphere as atmospheric ammonia (NH_{3gas}) under favorable conditions (Johnson et al., 2008; Carpenter et al., 2012; Paulot et al., 2015). The ocean is an important source of NH_{3gas}, contributing to approximately 40% of the natural NH₃ emissions on Earth (Carpenter et al., 2012; Paulot et al., 2015). In the literature, large uncertainties in the estimated NH₃ emissions from the ocean remain; for example, the annual emission flux ranges from 2 to 23 Tg N a⁻¹; (Clarke and Porter, 1993; Dentener and Crutzen, 1994; Sutton et al., 2013; Paulot et al., 2015). These uncertainties are primarily derived from two factors: 1) the major marine sources of NH_{3gas} are still disputed, such as seawater, sea-birds, or the photolysis of marine organic nitrogen at the ocean's surface or in the atmosphere; and 2) direct observations of NH_{3gas} in marine atmospheres are restricted as onboard ambient NH_{3gas} measurement techniques sometimes suffer from large artifacts due to NH_{3gas} contamination associated with onboard human activities, dew evaporation, and interference from water vapor. (Quinn et al., 1990; Clarke and Porter, 1993; Johnson et al., 2008; Keene et al., 2009; Wentworth et al., 2016; Teng et al., 2017) Additionally, the long-range transport of atmospheric NH_{3gas} from the continent may also complicate the source analysis of NH_{3gas} in marine atmospheres (McNaughton et al., 2004; Uematsu et al., 2004; Zhao et al., 2015; Lutsch et al., 2016).

To identify and characterize sea-derived gaseous amines, ammonia and sea-spray particulate aminium ions, as well as secondary particulate aminium ions from continental transport in the atmospheres of China's marginal seas, we conducted a cruise campaign over the Yellow and Bohai Seas in China from 9 to 22 December 2019 (Campaign A), and over the Eastern China and Yellow seas from December 27, 2019, to January 16, 2020 (Campaign B). Winter cruise campaigns provide great opportunities for observational studies due to the 1) higher concentration levels of nutrients in the seas at a lower sea surface water temperature (Guo et al., 2020); 2) periodically enhanced air-sea exchange driven by the strong winter Asian monsoon every 4–10 d (Zhu et al., 2018); and 3) periodically enhanced long-range transport of anthropogenic pollutants from continents to the seas (Guo et al., 2016; Wang et al., 2019).

In this study, an onboard URG-9000D Ambient Ion Monitor-Ion chromatography (AIM-IC, Thermo Fisher) was used to simultaneously measure the spatiotemporal variations in the concentrations of gaseous amines and NH_{3gas} with their counterparts in PM_{2.5}. Semi-continuous measurement data were then analyzed to identify the study targets. This study was divided into two parts. In this part, we focused on identifying marine sources from the continental transport of reduced



nitrogen compounds in marine atmospheres and subsequently quantified each contribution to the observed species during the
75 9-22 December 2019 campaign. In the companion paper (Gao et al., submitted to ACP), we analyzed the spatiotemporal
heterogeneity and related causes, and then delivered a hypothesis regarding the marine emissions of reduced nitrogen
compounds using the data obtained during the two campaigns and data from an additional cruise campaign previously
reported by Hu et al. (2015).

Experimental

80 Campaign A was conducted from December 9 to 19, 2019, on the R/V Dongfanghong-3 with a displacement tonnage of
5000 (Fig. 1). The research vessel was still within its testing period and used state-of-the-art combustion technology with
low-sulfur diesel. On December 19-22, the vessel was anchored at the port for Campaign B, organized by another research
team. A standard-sized air-conditioned container was set up on the front deck to house a suite of instruments for measuring
the air pollutant concentrations. No human activities occurred on the front deck during cruising, excluding anchoring at the
85 port. Even during the anchoring period, human activity on the front deck was rare. The use of the container on the front deck
effectively minimized self-vessel contamination by $\text{NH}_{3\text{gas}}$ and gaseous amines. The front deck was approximately 10 m
above sea-level, and the container height was 2.8 m.

To ensure that the onboard AIM-IC was operating properly, it was housed in a mobile air-conditioned mini-container, which
was further housed in a standard container with a 1-m stainless steel sampling probe connected to the ambient air. The inlet
90 of the sampling probe extended from the top corner of the standard container facing the sea. A $\text{PM}_{2.5}$ cyclone was installed
on the AIM-IC and operated at a rate of 3 L/min, which reports the semi-continuous concentrations of chemically reactive
gases, including $\text{NH}_{3\text{gas}}$, gaseous amines, and acidic gases such as SO_2 and HNO_3 , along with their particulate counterparts,
at a temporal resolution of 1 h, allowing the identification of possible interference from onboard dew evaporation, which
typically occurs with sunrise (Teng et al., 2017).

95 The AIM-IC includes an ICS-1100 ion chromatograph, in which an analytical column (Ion Pac CS17A (2×250 mm)) was
used to measure cations, including NH_4^+ , protonated dimethylamine (DMAH^+), and protonated trimethylamine (TMAH^+),
and an AG11-HC (2×50 mm) for measuring anions, including SO_4^{2-} , NO_3^- , Cl^- , and organic ions. The detection limits of



NH_4^+ , DMAH^+ , and TMAH^+ in the injection solution were 0.001, 0.008, and 0.001 mg/L, respectively. The ICS-1100 was calibrated onboard prior to the commencement of regular measurement collection, and the second calibration was conducted when the vessel was anchored at the port. The AIM-IC analysis was not affected by ambient water vapor as the device directly measured the ions. More detailed information regarding AIM-IC analysis is provided in the studies of Teng et al. (2017) and Xie et al., (2018). It should be noted that strong K^+ contamination unexpectedly occurred occasionally and then disappeared during different campaigns. When contamination occurred, DMAH^+ and TMAH^+ were undetectable due to the increased baseline at the corresponding residence time in the ion chromatograph; as such, some $\text{PM}_{2.5}$ DMAH^+ and TMAH^+ concentration data were unavailable in Fig 2. However, the concentrations of gaseous amines were still correctly detected with a low baseline at the residence. The K^+ contamination remains under investigation.

An automatic weather system that provides real-time meteorological data is available on the R/V Dongfanghong-3. The heading wind was corrected to determine the true wind speed and direction. The surface seawater temperature was not measured during this cruise campaign, and typically has a delay of a few hours when compared to the ambient air temperature (Deng et al., 2014). The NH_4^+ and aminium ion concentrations in the surface seawater were also not measured as the analytical methods are still hindered by high sea-salt ion contents.

On August 1-9 and September 12 to October 1, 2019, the AIM-IC was set up at a coastal site in Qingdao (36.34°N, 120.67°E) to collect routine measurements (Fig 2). The summer measurement data were obtained three to four months before the winter cruise campaign. The sampling site was located in a new high-technology zone near the Yellow Sea, with the shortest distance from the sea being approximately 1 km in the south. The AIM-IC was housed in a research lab on the fifth story of a building, approximately 16 m above ground-level. The sampling probe extended out of the window and was directly connected to the ambient air. Typically, higher biogenic emissions of reduced nitrogen compounds over the continents are expected in the summer than the winter due to the temperature effect (Yu et al., 2016; Teng et al., 2017).

3. Results

3.1 Temporal variations in the concentrations of basic gases and their $\text{PM}_{2.5}$ counterparts in the coastal atmosphere

Before analyzing the basic gases and their counterparts in the marine atmosphere, we first presented their continental



125 concentrations at the coastal site facing the Yellow Sea, as these observations provide important evidence to facilitate the analysis of the contributors to these species in the marine atmosphere. Figures 2a & b show that the TMA_{gas} and TMAH^+ concentrations in $\text{PM}_{2.5}$ always approached the detection limit, varying at approximately $0.002 \pm 0.001 \mu\text{g m}^{-3}$ (average \pm standard deviation), regardless of the presence of offshore or onshore winds. The DMA_{gas} and DMAH^+ concentrations varied at 0.017 ± 0.023 and $0.017 \pm 0.012 \mu\text{g m}^{-3}$, respectively, which were approximately one order of magnitude larger than those of TMA_{gas} and TMAH^+ . This suggests that the TMA_{gas} and TMAH^+ concentrations in the upwind continental and coastal atmospheres were extremely low. However, this was not the case—five to ten years ago. For example, the concentrations of the two aminium ions were comparable in atmospheric particles collected at two other coastal sites located approximately 20
130 km from the study area (Yu et al., 2016; Xie et al., 2018). The cause of this change is beyond the scope of this study, but may be the large decrease in manure application, based on our recent survey in the Qingdao area.

The DMA_{gas} and DMAH^+ in $\text{PM}_{2.5}$ concentrations with offshore winds were substantially higher than those with onshore winds, suggesting that their continental emissions and related secondary sources were stronger. Moreover, the concentrations of DMA_{gas} and DMAH^+ were moderately correlated with those of $\text{NH}_{3\text{gas}}$ and NH_4^+ , i.e., $[\text{DMA}_{\text{gas}}] = 5.1 \times 10^{-3} \times [\text{NH}_{3\text{gas}}]$ ($R^2=0.69$, $P<0.01$), and $[\text{DMAH}^+]_{\text{PM}_{2.5}} = 6.1 \times 10^{-3} \times [\text{NH}_4^+]_{\text{PM}_{2.5}}$ ($R^2=0.66$, $P<0.01$). Generally, the DMA_{gas} and DMAH^+ concentrations were approximately 1/200 of those of the corresponding $\text{NH}_{3\text{gas}}$ and NH_4^+ .
135

3.2 Spatiotemporal variations in the concentrations of basic gases over the seas

Throughout Campaign A, the TMA_{gas} concentrations varied at approximately $0.031 \pm 0.009 \mu\text{g m}^{-3}$ (Fig 1a-c), with three peaks occurring at 4- to 5-d intervals (gray shadowing in Fig. 1c). Peaks 1 and 2 were generally associated with offshore winds, while Peak 3 was mostly associated with onshore winds (Fig. 1b). The peaks lasted from tens to dozens of hours and were not caused by onboard dew evaporation at sunrise. For example, the highest value ($0.060 \mu\text{g m}^{-3}$) occurred at 23:00 on December 16. The observed concentrations were one order of magnitude higher than those measured in the coastal atmosphere during the summer. The values were also significantly higher than those of DMA_{gas} ($P<0.01$), which varied at approximately $0.006 \pm 0.006 \mu\text{g m}^{-3}$ (Fig 1d). The comparison results strongly indicated that the TMA_{gas} observed during
140
145 Campaign A was largely derived from marine sources. The same conclusion could be drawn by analyzing the three peaks of



150 TMA_{gas} and its temporal variations during the anchoring port period. For example, during Peak 1 (Fig. 1a), the concentrations of TMA_{gas} increased by approximately 100% from 20:00 on December 9 to 11:00 on December 10 with a decrease in the SO₄²⁻ concentration of approximately 30% (from 23 to 17 μg m⁻³; Fig 1b). Moreover, the peaks in the TMA_{gas} concentrations corresponded to troughs in the SO₄²⁻ concentrations during Peak 3, as shown in Figs 1c & d. The self-vessel emissions of SO₄²⁻ in PM_{2.5} were negligible due to the use of low-sulfur diesel, which will be discussed later. The increased SO₄²⁻ concentrations of PM_{2.5} may be a good indicator of continental transport, and vice versa.

155 Unlike TMA_{gas}, continental transport likely acted as an important contributor to the DMA_{gas} and NH_{3gas} observed in the marine atmosphere, particularly during Peak 1, when higher SO₄²⁻ concentrations were observed in PM_{2.5} (Figs 1c-e). The DMA_{gas} and NH_{3gas} concentrations were negatively correlated with those of TMA_{gas} during Peak 1, suggesting that most of the DMA_{gas} and NH_{3gas} were likely derived from continental transport, rather than marine sources. During Peak 2, increased TMA_{gas}, DMA_{gas}, and NH_{3gas} concentrations were observed concurrently with increasing SO₄²⁻ concentrations, suggesting that both the marine emissions and continental transport may contribute to the observed DMA_{gas} and NH_{3gas} at the same moment. During the port-anchoring period on 20-22 December, the DMA_{gas} and NH_{3gas} concentrations varied slightly, and were moderate and low, respectively. However, the TMA_{gas} concentrations continuously increased by over 100% as the ambient temperature increased (Figs 1c and f). Additionally, the SO₄²⁻ concentrations of PM_{2.5} varied greatly and followed a bell-shaped pattern during the port-anchoring period.

165 Additionally, the NH_{3gas} concentrations varied at approximately 0.53 ± 0.53 μg m⁻³ from December 9 to 22. The variation narrowed to approximately 0.24 ± 0.07 μg m⁻³ during the port-anchoring period on December 19-22. When the data during Campaign A were used for analysis, the NH_{3gas} concentrations were significantly correlated with those of DMA_{gas}; i.e., [DMA_{gas}] = 9.3 × 10⁻³ × [NH_{3gas}] (R²=0.35, P<0.01). However, there was no correlation between the NH_{3gas} and TMA_{gas} concentrations.

3.3 Spatiotemporal variations in the aminium and NH₄⁺ ion concentrations of PM_{2.5} over the seas

Figures 3a-f show the spatiotemporal variations in the TMAH⁺, DMAH⁺, and NH₄⁺ concentrations of PM_{2.5} throughout Campaign A from December 9 to 22, during which the TMAH⁺ concentrations varied greatly at approximately 0.28±0.18 μg



170 m^{-3} . However, they narrowed at approximately $0.21 \pm 0.04 \mu\text{g m}^{-3}$ during the port-anchoring period. The TMAH^+
concentrations generally increased from $0.13 \pm 0.05 \mu\text{g m}^{-3}$ on December 9 to $0.46 \pm 0.05 \mu\text{g m}^{-3}$ on December 16 (Fig. 3a),
and then decreased to approximately $0.2 \mu\text{g m}^{-3}$ afterward, excluding some strong peaks of $0.62\text{--}1.24 \mu\text{g m}^{-3}$ at 03:00–05:59
and $1.02\text{--}1.81 \mu\text{g m}^{-3}$ at 14:00–16:59 on 18 December (grey shadowing as Peak 4 in Figs 3a-d). The peaks reproduced the
episodes observed in the marine atmosphere over the Yellow Sea during May 2012 (Hu et al., 2015) and were repeatedly
175 observed during Campaign B (Gao et al., submitted to ACP), but were not observed in the several other marine cruise
campaigns conducted across the marginal seas of China and northwest Pacific Ocean (Hu et al., 2018; Xie et al., 2018).
As the TMAH^+ concentrations were approximately two orders of magnitude higher than the observations at the coastal site
during summer 2019, the observed TMAH^+ were likely largely derived from marine sources. The TMAH^+ concentrations
followed a spatiotemporal pattern that was clearly different from that of DMAH^+ and NH_4^+ , while the latter two ions
180 exhibited a similar spatiotemporal pattern during most of the periods throughout Campaign A (Figs 3a-c). A significant
negative correlation ($P < 0.01$) was obtained between the concentrations of TMAH^+ and NH_4^+ in $\text{PM}_{2.5}$ (not shown). The
spatiotemporal pattern of the TMAH^+ concentration was also greatly different to those of SO_4^{2-} (Fig. 1d) and SO_2 (Fig. 3b).
For example, the extremely strong TMAH^+ peaks occurred concurrently with low SO_4^{2-} , NH_4^+ , and SO_2 concentrations, while
accompanying with high concentrations of Na^+ under high wind speeds as indicators of sea spray aerosols (Feng et al., 2017).
185 Moreover, the TMAH^+ concentrations were approximately one order of magnitude larger than those of TMA_{gas} , and no
significant correlation was observed between them ($P > 0.05$). This suggests that the observed TMAH^+ may not be derived
from the neutralization reactions of TMA_{gas} with acids in the marine atmosphere, and may have been derived from primary
sea-spray organic aerosols (Ault et al., 2013; Prather et al., 2013; Quinn et al., 2015; Hu et al., 2018; Dall'Osto et al., 2019).
The DMAH^+ concentrations varied at approximately $0.065 \pm 0.068 \mu\text{g m}^{-3}$ on December 9-22; however, they varied at
190 approximately $0.10 \pm 0.04 \mu\text{g m}^{-3}$ during the port-anchoring period. The 25th percentile value of DMAH^+ during Campaign A
was $0.021 \mu\text{g m}^{-3}$, suggesting a low background concentration in the marine area. The DMAH^+ concentrations were
significantly correlated with those of NH_4^+ ($R^2 = 0.71$, $P < 0.01$; data not shown). When the data obtained at 03:00–05:59 and
14:00–16:59 on December 18 (strong peaks of TMAH^+ with a simultaneous increase in DMAH^+) were removed for
correlation, the R^2 value improved to 0.78. Unlike the TMAH^+ , the observed DMAH^+ may have been partially derived from



195 acid-basic neutralization reactions in ambient air, in addition to the primary sea-spray organic aerosols. For example, largely increased DMAH⁺ concentrations occurred concurrently with strong peaks in the TMAH⁺ concentrations (gray shadowed peak 4 in Figs 3a & b).

The NH₄⁺ concentrations of PM_{2.5} varied greatly at approximately $4.7 \pm 7.2 \mu\text{g m}^{-3}$ during Campaign A (Fig. 3c). However, the 25th percentile values were as low as $0.21 \mu\text{g m}^{-3}$, suggesting low marine background values. The 50th percentile value
200 was also only $1.2 \mu\text{g m}^{-3}$, which was much smaller than the average value due to the presence of strong peaks in the NH₄⁺ concentrations. The increased NH₄⁺ concentrations associated with NO₃⁻ and SO₄²⁻ during Campaign A were likely due to long-range transport from the upwind continents.

4. Discussion

4.1 Effects of temperature on the observed basic gases in the marine atmosphere

205 As mentioned above, the observed TMA_{gas} likely originated from marine sources. We plotted the concentrations of TMA_{gas} against the ambient air temperature (T) in Fig. 4a, which generally increased with increasing T. We further separated the average hourly wind speeds (WS) into three categories, i.e., $WS \leq 5.0$, $5.0 < WS \leq 9.0$, and $WS > 9.0 \text{ m s}^{-1}$. At $WS > 9.0 \text{ m s}^{-1}$, the data obtained from 15:00 on December 16 to 01:00 on December 19 including Peaks 3 and 4, were separately considered as half-full symbols in Fig. 4a. The TMA_{gas} concentrations (half-full symbols) generally exceeded the concentrations of the
210 other gases at the same T, with which they exhibited a moderately good exponent correlation, ($[\text{TMA}_{\text{gas}}] = 0.03 \times e^{0.04T}$ with $R^2=0.72$). From 15:00 on December 16 to 01:00 on December 19 stronger emission potentials of TMA_{gas} to the marine atmosphere were expected in the corresponding marine zone. Although the TMAH⁺ in the surface seawater was not directly measured, higher TMAH⁺ concentrations were expected.

Following the same approach, the DMA_{gas} and NH_{3gas} concentrations were plotted against T, as shown in Figs 4b & c,
215 respectively. They generally increased with increasing T. The NH_{3gas} concentrations (half-full symbols) were extremely well correlated with T ($[\text{NH}_{3\text{gas}}] = 0.05 \times e^{0.3T}$ with $R^2=0.96$). As lower concentrations of SO₄²⁻, NH₄⁺, and SO₂ were generally observed at the same time, the continental transport of NH_{3gas} should be greatly reduced; therefore, the observed NH_{3gas} was likely mainly derived from the seas. Therefore, the seas were the net source of NH_{3gas} at the measurement time. However, at



the same T, the $\text{NH}_{3\text{gas}}$ concentrations (half-full symbols) were generally lower than those during the other periods in this study. The concentrations of NH_4^+ in the surface seawater may have been lower at the measurement time. However, this may not be the case as higher concentrations of TMAH^+ were expected. Alternatively, the continental transport of $\text{NH}_{3\text{gas}}$ may have made an important contribution to the observed $\text{NH}_{3\text{gas}}$ during most of the other periods when the seas were the net $\text{NH}_{3\text{gas}}$ sink.

DMA_{gas} exhibited an extremely good exponent correlation with T (half-full symbols) at the measurement time ($[\text{NH}_{3\text{gas}}] = 0.002 \times e^{0.3T}$ with $R^2=0.93$). At the same T, the DMA_{gas} concentrations (half-full symbols) were not always higher or lower than the others. Two scenarios were considered. Under Scenario 1, the observed DMA_{gas} concentrations exceeded the values predicted by the regression equation using the ambient T as the input. The seas were the likely net sinks of the DMA_{gas} . Under Scenario 2, including all others, measurements of the DMAH^+ in the surface seawater were required to confirm whether the seas were the net sources or sinks of DMA_{gas} .

4.2 Estimating sea-derived DMA_{gas} and $\text{NH}_{3\text{gas}}$ in the marine atmosphere

To estimate the sea-derived DMA_{gas} and $\text{NH}_{3\text{gas}}$ concentrations in the marine atmosphere, we plotted the DMA_{gas} and $\text{NH}_{3\text{gas}}$ concentrations against TMA_{gas} , as shown in Figs 5a & b. The purple-red and dark-green markers represent the data obtained during the increasing and decreasing periods of Peak 3, respectively, which were analyzed separately. A good correlation can be obtained between DMA_{gas} and TMA_{gas} during the increasing period ($[\text{DMA}_{\text{gas}}] = 0.63 \times [\text{TMA}_{\text{gas}}] - 0.01$, $R^2=0.89$ and $P<0.01$). The equation for the decreasing period was as follows: $[\text{DMA}_{\text{gas}}] = 1.3 \times [\text{TMA}_{\text{gas}}] - 0.05$, $R^2=0.79$ and $P<0.01$. Therefore, the TMAH^+ in the surface seawater may decompose into DMAH^+ to different extents (Lidbury et al., 2015a; Lidbury et al., 2015b; Xie et al., 2018). The two regression curves (purple-red and dark-green dashed lines in Figs 5a & b) created a large triangular zone that likely reflected the different ratios of $\text{DMA}_{\text{gas}}/\text{TMA}_{\text{gas}}$ in primary marine emissions. We assumed that any data beyond the purple-red dashed line reflected the contribution of non-sea-derived DMA_{gas} , which should be attributed to continental transport. Therefore, we assumed that the non-sea-derived DMA_{gas} ($\text{DMA}_{\text{gas}}^\#$) concentrations were equal to the observed values of DMA_{gas} minus the predicted values obtained using $[\text{DMA}_{\text{gas}}] = 0.63 \times [\text{TMA}_{\text{gas}}] - 0.01$, and the calculated $\text{DMA}_{\text{gas}}^\#$ values are shown in Fig. 5c. Based on the triangular zone in Fig. 5a, the calculated values should



be considered as the lower limit of $\text{DMA}_{\text{gas}}^{\#}$. During Peak 1, the calculated $\text{DMA}_{\text{gas}}^{\#}$ contributed to over 40% of the observed DMA_{gas} for 12 h. Similar calculated results for $\text{DMA}_{\text{gas}}^{\#}$ were obtained during Peak 2.

245 The same approach was employed to analyze the $\text{NH}_{3\text{gas}}$ results, as shown in Figs 5b and d. During Peak 1, the calculated non-sea-derived $\text{NH}_{3\text{gas}}$ ($\text{NH}_{3\text{gas}}^{\#}$) contributed to over 40% of the observed $\text{NH}_{3\text{gas}}$ for 17 h. During Peak 2, the calculated $\text{NH}_{3\text{gas}}^{\#}$ contributed to over 40% of the observed $\text{NH}_{3\text{gas}}$ for 24 h.

Overall, the $\text{DMA}_{\text{gas}}^{\#}$ and $\text{NH}_{3\text{gas}}^{\#}$ concentrations varied at approximately 0.001 ± 0.003 and $0.18\pm 0.39 \mu\text{g m}^{-3}$, respectively. The calculated average $\text{DMA}_{\text{gas}}^{\#}$ and $\text{NH}_{3\text{gas}}^{\#}$ values accounted for 16% and 34% of the observed averages of each species, respectively.

250

4.3 Estimation of non-sea-spray particulate DMAH^+ in the marine atmosphere

We plotted the concentrations of DMAH^+ against those of TMAH^+ in $\text{PM}_{2.5}$ (Fig. 6a) using the data obtained from 15:00 on December 16 to 01:00 on December 19 ($[\text{DMAH}^+]_{\text{PM}_{2.5}} = 0.13 \times [\text{TMAH}^+]_{\text{PM}_{2.5}}$, $R^2=0.91$, $P<0.01$). We assumed that the non-sea-primarily derived DMAH^+ concentrations in $\text{PM}_{2.5}$, marked as $\text{DMAH}^{\#}$, were equal to the observed DMAH^+ values minus the predicted values using the regression equation. The calculated $\text{DMAH}^{\#}$ values are shown in Fig. 6b. The $\text{DMAH}^{\#}$ concentrations varied at approximately $0.042\pm 0.070 \mu\text{g m}^{-3}$ throughout Campaign A, during which the calculated average $\text{DMAH}^{\#}$ accounted for 65% of the observed average. Additionally, the calculated $\text{DMAH}^{\#}$ values accounted for over 80% of the observed values in 26% of the Campaign-A period. Again, the decomposition of TMAH^+ to DMAH^+ may have occurred in surface seawater and/or the marine atmosphere, to an extent, and the estimated $\text{DMAH}^{\#}$ should be considered as the upper limit. Note that the NH_4^+ and TMAH^+ concentrations were negatively correlated during Campaign A, and no primary particulate NH_4^+ from sea-spray aerosols could be identified.

255

260

When the concentrations of $\text{DMAH}^{\#}$ were plotted against those of NH_4^+ (Fig 6c), we obtained the following equation: $[\text{DMAH}^{\#}]_{\text{PM}_{2.5}} = 0.0089 \times [\text{NH}_4^+]_{\text{PM}_{2.5}}$, $R^2=0.82$, $P<0.01$. The slope was larger than that obtained in the coastal atmosphere during the summer (0.0061). This difference may be partially explained by the gas-aerosol equilibria among them (Pankow, 2015; Xie et al., 2018), considering the two regression equations, i.e., $[\text{DMA}_{\text{gas}}] = 9.3 \times 10^{-3} \times [\text{NH}_{3\text{gas}}]$ in the marine atmosphere, and $[\text{DMA}_{\text{gas}}] = 5.1 \times 10^{-3} \times [\text{NH}_{3\text{gas}}]$ in the summer coastal atmosphere.

265



4.4 Formation and chemical conversion of aminium ions in the transported and self-vessel SO₂ plumes

When the sea-spray particulate DMAH⁺ was deducted, the increased concentrations of DMAH⁺⁺ were generally associated with increased SO₄²⁻ and SO₂ concentrations. Combining this with the moderate correlation between DMAH⁺⁺ and NH₄⁺, it can be inferred that the DMAH⁺⁺ likely originated from concurrent secondary formation with NH₄⁺. However, we separated the air pollutant plumes into two groups. Group 1 represented an increase in SO₄²⁻ and NH₄⁺ together with SO₂, while Group 2 represented an increase in SO₂ without increases in SO₄²⁻ and NH₄⁺. Group 1 likely reflected the transport of aged air pollutant plumes from the continents, while Group 2 may reflect self-vessel SO₂ plumes. As shown in Figs 6b and 3b-c, the concentrations of DMAH⁺⁺ and NH₄⁺ in the self-vessel SO₂ plumes did not increase in the intervals between Peaks 1 and 2, and between Peaks 2 and 3. Therefore, no fresh formation of DMAH⁺⁺ and NH₄⁺ in the self-vessel emissions was detected. However, the concentrations of TMAH⁺ decreased in some self-vessel SO₂ plumes. The TMAH⁺ concentrations were approximately one order of magnitude higher than those of TMA_{gas} in the marine atmosphere. Assuming that the decreased TMAH⁺ was released from PM_{2.5} to the gas phase, a simultaneous large spike in TMA_{gas} should be observed. However, this was not the case, as shown in Fig 1c. The decreased TMAH⁺ may persist in the PM_{2.5}, but could not be detected by AIM-IC.

4. Conclusion and Implication

In continental China upwind of the Yellow Sea, the TMA_{gas} and TMAH⁺ concentrations in PM_{2.5} were extremely low (0.002±0.001 μg m⁻³), close to the detection limit of the AIM-IC. Taking the observations as a reference, the largely increased TMA_{gas} (0.031±0.009 μg m⁻³) and particulate TMAH⁺ (0.28±0.18 μg m⁻³) concentrations in the marine atmosphere were attributed to marine emissions. Therefore, TMA_{gas} and particulate TMAH⁺ can be used as unique tracers to quantify the marine emissions of DMA_{gas}, NH_{3gas}, and particulate DMAH⁺, as well as the long-range transport from upwind continental China.

Through comprehensive comparison and correlation analyses, the high concentrations of TMAH⁺ in PM_{2.5} observed over the Yellow and Bohai Seas, with episodic average hourly exceeding over 1 μg m⁻³, were inferred to originate from strong primary sea-spray aerosol emissions. Moreover, the TMA_{gas} concentrations generally increased with increasing ambient temperature and sea surface wind speeds, suggesting that the observed TMA_{gas} was likely released from the surface seawater.



However, the TMA_{gas} concentrations were substantially lower than those of particulate TMAH^+ , and were not significantly correlated. Although different mechanisms of the release of TMA_{gas} and particulate TMAH^+ from the seas have been reported in the literature, the lack of a significant correlation between them was surprising and is explored in the companion study.

295 The DMA_{gas} and $\text{NH}_{3\text{gas}}$ concentrations varied at approximately 0.006 ± 0.006 and $0.53 \pm 0.53 \mu\text{g m}^{-3}$ during Campaign A, in which at least 16% and 34 % of the observational values were derived from continental transport, respectively. The sea-derived DMA_{gas} and $\text{NH}_{3\text{gas}}$ were likely released with TMA_{gas} as they peaked simultaneously. The DMAH^+ concentrations of $\text{PM}_{2.5}$ varied at approximately $0.065 \pm 0.068 \mu\text{g m}^{-3}$ during Campaign A, 65% of which was derived from continental transport.

300 Our analysis results did not support the occurrence of the photolysis of marine organic nitrogen to generate $\text{NH}_{3\text{gas}}$ in the marine atmosphere during winter as there was no correlation between the sea-derived $\text{NH}_{3\text{gas}}$ and particulate TMAH^+ concentrations. Additionally, Peaks 2 and 3 of $\text{NH}_{3\text{gas}}$ persisted for dozens of hours under strong winds and were unlikely to be derived from seabird emissions. Alternatively, a good exponent correlation was observed between the observed $\text{NH}_{3\text{gas}}$ concentrations and T during the period lacking continental air pollutant transport, suggesting that the observed $\text{NH}_{3\text{gas}}$ was released from seawater. NH_3 emissions via seabirds were unlikely to be an important contributor to the observed $\text{NH}_{3\text{gas}}$ in the marine atmosphere during winter, although this may not have been the case during other seasons.

305 Additionally, no formation of particulate NH_4^+ and DMAH^+ in the self-vessel SO_2 plume was observed in the marine atmosphere. However, the particulate TMAH^+ concentration clearly decreased in the self-vessel SO_2 plume without a simultaneous increase in the TMA_{gas} concentrations. Undetectable chemical conversion of particulate TMAH^+ by AIM-IC likely occurred and requires further investigation.

Data availability. The data of this paper are available upon request (contact: Xiaohong Yao, xhyao@ouc.edu.cn).

Acknowledgment

This research is supported by the National Key Research and Development Program in China (grant no. 2016YFC0200504), the Natural Science Foundation of China (grant no. 41776086)



315 References

- Almeida, J., Schobesberger, S., Kürten, A., Ortega, I. K., Kupiainen-Määttä, O., Praplan, A. P., Adamov, A., Amorim, A., Bianchi, F., Breitenlechner, M., David, A., Dommen, J., Donahue, N. M., Downard, A., Dunne, E., Duplissy, J., Ehrhart, S., Flagan, R. C., Franchin, A., Guida, R., Hakala, J., Hansel, A., Heinritzi, M., Henschel, H., Jokinen, T., Junninen, H., Kajos, M., Kangasluoma, J., Keskinen, H., Kupc, A., Kurtén, T., Kvashin, A. N., Laaksonen, A., Lehtipalo, K., Leiminger, M., Leppä, J., Loukonen, V., Makhmutov, V., Mathot, S., McGrath, M. J., Nieminen, T., Olenius, T., Onnela, A., Petäjä, T., Riccobono, F., Riipinen, I., Rissanen, M., Rondo, L., Ruuskanen, T., Santos, F. D., Sarnela, N., Schallhart, S., Schnitzhofer, R., Seinfeld, J. H., Simon, M., Sipilä, M., Stozhkov, Y., Stratmann, F., Tomé, A., Tröstl, J., Tsagkogeorgas, G., Vaattovaara, P., Viisanen, Y., Virtanen, A., Vrtala, A., Wagner, P. E., Weingartner, E., Wex, H., Williamson, C., Wimmer, D., Ye, P., Yli-Juuti, T., Carslaw, K. S., Kulmala, M., Curtius, J., Baltensperger, U., Worsnop, D. R., Vehkamäki, H., and Kirkby, J.: Molecular understanding of sulphuric acid–amine particle nucleation in the atmosphere, *Nature*, 502, 359–363, <https://doi.org/10.1038/nature12663>, 2013.
- Ault, A. P., Moffet, R. C., Baltusaitis, J., Collins, D. B., Ruppel, M. J., Cuadra-Rodriguez, L. A., Zhao, D., Guasco, T. L., Ebben, C. J., Geiger, F. M., Bertram, T. H., Prather, K. A., and Grassian, V. H.: Size-dependent changes in sea spray aerosol composition and properties with different seawater conditions, *Environmental Science & Technology*, 47, 5603–5612, <https://doi.org/10.1021/es400416g>, 2013.
- Burg, M. B. and Ferraris, J. D.: Intracellular organic osmolytes: Function and regulation, *Journal of Biological Chemistry*, 283, 7309–7313, <https://doi.org/10.1074/jbc.R700042200>, 2008.
- Carpenter, L. J., Archer, S. D., and Beale, R.: Ocean-atmosphere trace gas exchange, *Chem. Soc. Rev.*, 41, 6473–6506, <https://doi.org/10.1039/C2CS35121H>, 2012.
- Chen, H., Varner, M. E., Gerber, R. B., and Finlayson-Pitts, B. J.: Reactions of methanesulfonic acid with amines and ammonia as a source of new particles in air, *The Journal of Physical Chemistry B*, 120, 1526–1536, <https://doi.org/10.1021/acs.jpcc.5b07433>, 2016.
- Clarke, A. D. and Porter, J. N.: Pacific marine aerosol: 2. Equatorial gradients in chlorophyll, ammonium, and excess sulfate during SAGA 3, *J. Geophys. Res.*, 98, 16997–17010, <https://doi.org/10.1029/92JD02481>, 1993.



- 340 Dall'Osto, M., Airs, R. L., Beale, R., Cree, C., Fitzsimons, M. F., Beddows, D., Harrison, R. M., Ceburnis, D., O'Dowd, C.,
Rinaldi, M., Paglione, M., Nenes, A., Decesari, S., and Simó, R.: Simultaneous detection of alkylamines in the surface
ocean and atmosphere of the Antarctic sympagic environment, *ACS Earth and Space Chemistry*, 3, 854–862,
<https://doi.org/10.1021/acsearthspacechem.9b00028>, 2019.
- Deng, Y., Gao, T., Gao, H., Yao, X., and Xie, L.: Regional precipitation variability in East Asia related to climate and
345 environmental factors during 1979–2012, *Sci Rep*, 4, 5693, <https://doi.org/10.1038/srep05693>, 2014.
- Dentener, F. J. and Crutzen, P. J.: A three-dimensional model of the global ammonia cycle, *Journal of Atmospheric
Chemistry*, 19, 331–369, <https://doi.org/10.1007/BF00694492>, 1994.
- Facchini, M. C., Decesari, S., Rinaldi, M., Carbone, C., Finessi, E., Mircea, M., Fuzzi, S., Moretti, F., Tagliavini, E.,
Ceburnis, D., and O'Dowd, C. D.: Important source of marine secondary organic aerosol from biogenic amines,
350 *Environmental Science & Technology*, 42, 9116–9121, <https://doi.org/10.1021/es8018385>, 2008.
- Feng, L., Shen, H., Zhu, Y., Gao, H., and Yao, X.: Insight into generation and evolution of sea-salt aerosols from field
measurements in diversified marine and coastal atmospheres, *Scientific Reports*, 7, 41260,
<https://doi.org/10.1038/srep41260>, 2017.
- Gao, Y., Chen, D., Shen, Y., Gao, Y., Gao, H., and Yao, X.: Semi-continuous observations of gaseous amines and ammonia
355 and particulate counterparts in winter marine atmospheres over marginal seas of China: Spatiotemporal heterogeneity,
controlling factor and new hypothesis (2), submitted to *ACP*
- Guo, C., Zhang, G., Sun, J., Leng, X., Xu, W., Wu, C., Li, X., and Pujari, L.: Seasonal responses of nutrient to hydrology
and biology in the southern Yellow Sea, *Continental Shelf Research*, 206, 104207,
<https://doi.org/10.1016/j.csr.2020.104207>, 2020.
- 360 Guo, T., Li, K., Zhu, Y., Gao, H., and Yao, X.: Concentration and size distribution of particulate oxalate in marine and
coastal atmospheres – Implication for the increased importance of oxalate in nanometer atmospheric particles,
Atmospheric Environment, 142, 19–31, <https://doi.org/10.1016/j.atmosenv.2016.07.026>, 2016.
- Hu, Q., Qu, K., Gao, H., Cui, Z., Gao, Y., and Yao, X.: Large increases in primary trimethylaminium and secondary
dimethylaminium in atmospheric particles associated with cyclonic eddies in the northwest Pacific Ocean, *Journal of*



- 365 Geophysical Research: Atmospheres, 123, 12,133-12,146, <https://doi.org/10.1029/2018JD028836>, 2018.
- Hu, Q., Yu, P., Zhu, Y., Li, K., Gao, H., and Yao, X.: Concentration, size distribution, and formation of trimethylammonium and dimethylammonium ions in atmospheric particles over marginal seas of China, *Journal of the Atmospheric Sciences*, 72, 3487–3498, <https://doi.org/10.1175/JAS-D-14-0393.1>, 2015.
- Jameson, E., Doxey, A. C., Airs, R., Purdy, K. J., Murrell, J. C., and Chen, Y.: Metagenomic data-mining reveals contrasting
370 microbial populations responsible for trimethylamine formation in human gut and marine ecosystems, *Microbial Genomics*, 2, <https://doi.org/10.1099/mgen.0.000080>, 2016.
- Johnson, M. T., Liss, P. S., Bell, T. G., Lesworth, T. J., Baker, A. R., Hind, A. J., Jickells, T. D., Biswas, K. F., Woodward, E. M. S., and Gibb, S. W.: Field observations of the ocean-atmosphere exchange of ammonia: Fundamental importance of temperature as revealed by a comparison of high and low latitudes, *Global Biogeochem. Cycles*, 22,
375 <https://doi.org/10.1029/2007GB003039>, 2008.
- Keene, W. C., Long, M. S., Pszenny, A. A. P., Sander, R., Maben, J. R., Wall, A. J., O’Halloran, T. L., Kerkweg, A., Fischer, E. V., and Schrems, O.: Latitudinal variation in the multiphase chemical processing of inorganic halogens and related species over the eastern North and South Atlantic Oceans, *Atmospheric Chemistry and Physics*, 9, 7361–7385, <https://doi.org/10.5194/acp-9-7361-2009>, 2009.
- 380 Lidbury, I., Kimberley, G., Scanlan, D. J., Murrell, J. C., and Chen, Y.: Comparative genomics and mutagenesis analyses of choline metabolism in the marine *Roseobacter* clade, *Environ Microbiol*, 17, 5048–5062, <https://doi.org/10.1111/1462-2920.12943>, 2015a.
- Lidbury, I. D., Murrell, J. C., and Chen, Y.: Trimethylamine and trimethylamine N-oxide are supplementary energy sources for a marine heterotrophic bacterium: Implications for marine carbon and nitrogen cycling, *The ISME Journal*, 9, 760–
385 769, <https://doi.org/10.1038/ismej.2014.149>, 2015b.
- Lutsch, E., Dammers, E., Conway, S., and Strong, K.: Long-range transport of NH₃, CO, HCN, and C₂H₆ from the 2014 Canadian wildfires, *Geophysical Research Letters*, 43, 8286–8297, <https://doi.org/10.1002/2016GL070114>, 2016.
- McNaughton, C. S., Clarke, A. D., Howell, S. G., Moore II, K. G., Brekhovskikh, V., Weber, R. J., Orsini, D. A., Covert, D. S., Buzorius, G., Brechtel, F. J., Carmichael, G. R., Tang, Y., Eisele, F. L., Mauldin, R. L., Bandy, A. R., Thornton, D.



- 390 C., and Blomquist, B.: Spatial distribution and size evolution of particles in Asian outflow: Significance of primary and secondary aerosols during ACE-Asia and TRACE-P, *Journal of Geophysical Research: Atmospheres*, 109, <https://doi.org/10.1029/2003JD003528>, 2004.
- Müller, C., Iinuma, Y., Karstensen, J., van Pinxteren, D., Lehmann, S., Gnauk, T., and Herrmann, H.: Seasonal variation of aliphatic amines in marine sub-micrometer particles at the Cape Verde islands, *Atmospheric Chemistry and Physics*, 9, 9587–9597, <https://doi.org/10.5194/acp-9-9587-2009>, available at: <https://acp.copernicus.org/articles/9/9587/2009/>, 2009.
- Pankow, J. F.: Phase considerations in the gas/particle partitioning of organic amines in the atmosphere, *Atmospheric Environment*, 122, 448–453, <https://doi.org/10.1016/j.atmosenv.2015.09.056>, 2015.
- Paulot, F., Jacob, D. J., Johnson, M. T., Bell, T. G., Baker, A. R., Keene, W. C., Lima, I. D., Doney, S. C., and Stock, C. A.: 400 Global oceanic emission of ammonia: Constraints from seawater and atmospheric observations, *Global Biogeochem. Cycles*, 29, 1165–1178, <https://doi.org/10.1002/2015GB005106>, 2015.
- Prather, K. A., Bertram, T. H., Grassian, V. H., Deane, G. B., Stokes, M. D., Demott, P. J., Aluwihare, L. I., Palenik, B. P., Azam, F., Seinfeld, J. H., Moffet, R. C., Molina, M. J., Cappa, C. D., Geiger, F. M., Roberts, G. C., Russell, L. M., Ault, A. P., Baltrusaitis, J., Collins, D. B., Corrigan, C. E., Cuadra-Rodriguez, L. A., Ebben, C. J., Forestieri, S. D., Guasco, T. 405 L., Hersey, S. P., Kim, M. J., Lambert, W. F., Modini, R. L., Mui, W., Pedler, B. E., Ruppel, M. J., Ryder, O. S., Schoepp, N. G., Sullivan, R. C., and Zhao, D.: Bringing the ocean into the laboratory to probe the chemical complexity of sea spray aerosol, *Proc Natl Acad Sci U S A*, 110, 7550–7555, <https://doi.org/10.1073/pnas.1300262110>, 2013.
- Quinn, P. K., Collins, D. B., Grassian, V. H., Prather, K. A., and Bates, T. S.: Chemistry and related properties of freshly emitted sea spray aerosol, *Chemical Reviews*, 115, 4383–4399, <https://doi.org/10.1021/cr500713g>, 2015.
- 410 Quinn, P. K., Bates, T. S., Johnson, J. E., Covert, D. S., and Charlson, R. J.: Interactions between the sulfur and reduced nitrogen cycles over the central Pacific Ocean, *J. Geophys. Res.*, 95, 16405–16416, <https://doi.org/10.1029/JD095iD10p16405>, 1990.
- Sutton, M. A., Reis, S., Riddick, S. N., Dragosits, U., Nemitz, E., Theobald, M. R., Tang, Y. S., Braban, C. F., Vieno, M., Dore, A. J., Mitchell, R. F., Wanless, S., Daunt, F., Fowler, D., Blackall, T. D., Milford, C., Flechard, C. R., Loubet, B.,



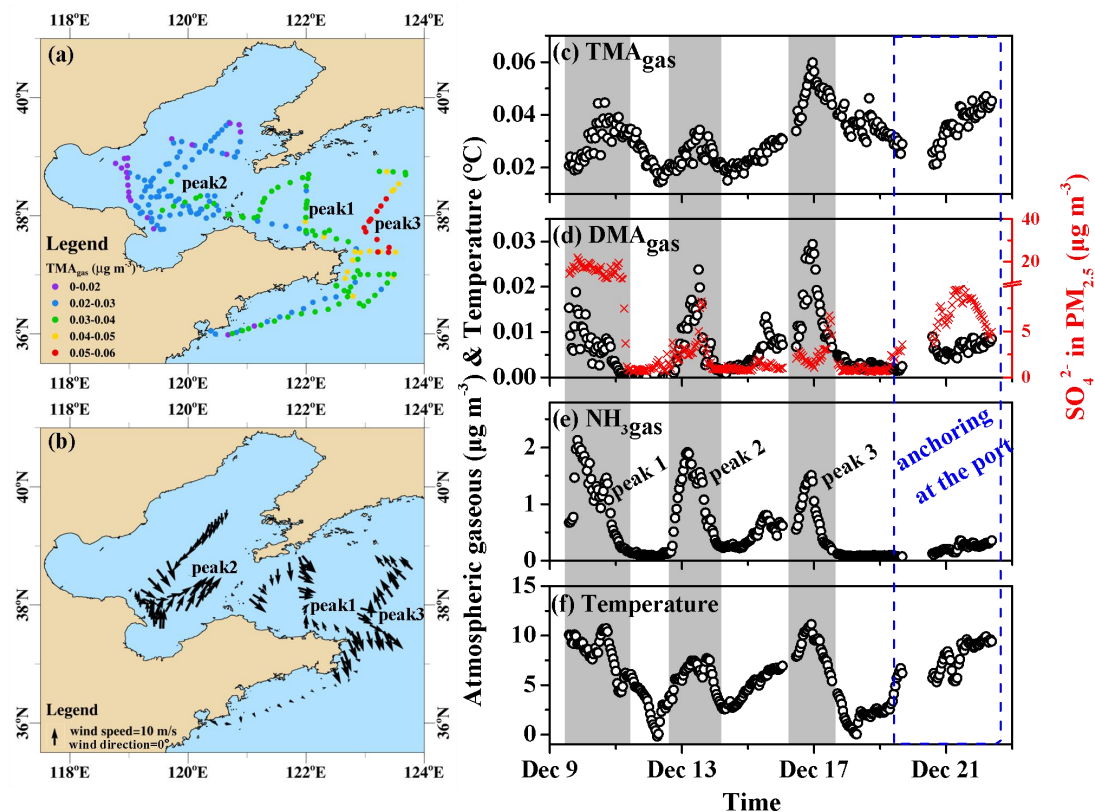
- 415 Massad, R., Cellier, P., Personne, E., Coheur, P. F., Clarisse, L., van Damme, M., Ngadi, Y., Clerbaux, C., Skjøth, C. A.,
Geels, C., Hertel, O., Wichink Kruit, R. J., Pinder, R. W., Bash, J. O., Walker, J. T., Simpson, D., Horváth, L.,
Misselbrook, T. H., Bleeker, A., Dentener, F., and Vries, W. de: Towards a climate-dependent paradigm of ammonia
emission and deposition, *Philosophical Transactions of the Royal Society B: Biological Sciences*, 368, 20130166,
<https://doi.org/10.1098/rstb.2013.0166>, 2013.
- 420 Taubert, M., Grob, C., Howat, A. M., Burns, O. J., Pratscher, J., Jehmlich, N., Bergen, M. von, Richnow, H. H., Chen, Y.,
and Murrell, J. C.: Methylamine as a nitrogen source for microorganisms from a coastal marine environment, *Environ
Microbiol*, 19, 2246–2257, <https://doi.org/10.1111/1462-2920.13709>, 2017.
- Teng, X., Hu, Q., Zhang, L., Qi, J., Shi, J., Xie, H., Gao, H., and Yao, X.: Identification of major sources of atmospheric
NH₃ in an urban environment in northern China during wintertime, *Environmental Science & Technology*, 51, 6839–
425 6848, <https://doi.org/10.1021/acs.est.7b00328>, 2017.
- Uematsu, M., Toratani, M., Kajino, M., Narita, Y., Senga, Y., and Kimoto, T.: Enhancement of primary productivity in the
western North Pacific caused by the eruption of the Miyake-jima Volcano, *Geophysical Research Letters*, 31,
<https://doi.org/10.1029/2003GL018790>, 2004.
- van Pinxteren, M., Fomba, K. W., van Pinxteren, D., Triesch, N., Hoffmann, E. H., Cree, C. H.L., Fitzsimons, M. F.,
430 Tümpling, W. von, and Herrmann, H.: Aliphatic amines at the Cape Verde Atmospheric Observatory: Abundance,
origins and sea-air fluxes, *Atmospheric Environment*, 203, 183–195, <https://doi.org/10.1016/j.atmosenv.2019.02.011>,
2019.
- van Pinxteren, M., Fiedler, B., van Pinxteren, D., Iinuma, Y., Körtzinger, A., and Herrmann, H.: Chemical characterization
of sub-micrometer aerosol particles in the tropical Atlantic Ocean: Marine and biomass burning influences, *Journal of*
435 *Atmospheric Chemistry*, 72, 105–125, <https://doi.org/10.1007/s10874-015-9307-3>, 2015.
- VandenBoer, T. C., Petroff, A., Markovic, M. Z., and Murphy, J. G.: Size distribution of alkyl amines in continental
particulate matter and their online detection in the gas and particle phase, *Atmospheric Chemistry and Physics*, 11,
4319–4332, <https://doi.org/10.5194/acp-11-4319-2011>, 2011.
- Wang, B., Chen, Y., Zhou, S., Li, H., Wang, F., and Yang, T.: The influence of terrestrial transport on visibility and aerosol



- 440 properties over the coastal East China Sea, *Science of The Total Environment*, 649, 652–660,
<https://doi.org/10.1016/j.scitotenv.2018.08.312>, 2019.
- Wentworth, G. R., Murphy, J. G., Benedict, K. B., Bangs, E. J., and Collett Jr., J. L.: The role of dew as a night-time
reservoir and morning source for atmospheric ammonia, *Atmospheric Chemistry and Physics*, 16, 7435–7449,
<https://doi.org/10.5194/acp-16-7435-2016>, 2016.
- 445 Xie, H., Feng, L., Hu, Q., Zhu, Y., Gao, H., Gao, Y., and Yao, X.: Concentration and size distribution of water-extracted
dimethylammonium and trimethylammonium in atmospheric particles during nine campaigns - Implications for sources,
phase states and formation pathways, *Science of The Total Environment*, 631–632, 130–141,
<https://doi.org/10.1016/j.scitotenv.2018.02.303>, 2018.
- Yao, L., Garmash, O., Bianchi, F., Zheng, J., Yan, C., Kontkanen, J., Junninen, H., Mazon, S. B., Ehn, M., Paasonen, P.,
450 Sipilä, M., Wang, M., Wang, X., Xiao, S., Chen, H., Lu, Y., Zhang, B., Wang, D., Fu, Q., Geng, F., Li, L., Wang, H.,
Qiao, L., Yang, X., Chen, J., Kerminen, V.-M., Petäjä, T., Worsnop, D. R., Kulmala, M., and Wang, L.: Atmospheric
new particle formation from sulfuric acid and amines in a Chinese megacity, *Science*, 361, 278–281,
<https://doi.org/10.1126/science.aao4839>, 2018.
- Yu, P., Hu, Q., Li, K., Zhu, Y., Liu, X., Gao, H., and Yao, X.: Characteristics of dimethylammonium and trimethylammonium in
455 atmospheric particles ranging from supermicron to nanometer sizes over eutrophic marginal seas of China and
oligotrophic open oceans, *Science of The Total Environment*, 572, 813–824,
<https://doi.org/10.1016/j.scitotenv.2016.07.114>, 2016.
- Zhao, Y., Zhang, L., Pan, Y., Wang, Y., Paulot, F., and Henze, D. K.: Atmospheric nitrogen deposition to the northwestern
Pacific: seasonal variation and source attribution, *Atmospheric Chemistry and Physics*, 15, 10905–10924,
460 <https://doi.org/10.5194/acp-15-10905-2015>, 2015.
- Zhou, S., Li, H., Yang, T., Chen, Y., Deng, C., Gao, Y., Chen, C., and Xu, J.: Characteristics and sources of aerosol
ammoniums over the eastern coast of China: Insights from the integrated observations in a coastal city, adjacent island and
surrounding marginal seas, *Atmospheric Chemistry and Physics*, 19, 10447–10467, <https://doi.org/10.5194/acp-19-10447-2019>, 2019.



- 465 Zhu, J., Shi, J., Guo, X., Gao, H., and Yao, X.: Air-sea heat flux control on the Yellow Sea Cold Water Mass intensity and implications for its prediction, *Continental Shelf Research*, 152, 14–26, <https://doi.org/10.1016/j.csr.2017.10.006>, 2018.
- Zhu, Y., Li, K., Shen, Y., Gao, Y., Liu, X., Yu, Y., Gao, H., and Yao, X.: New particle formation in the marine atmosphere during seven cruise campaigns, *Atmospheric Chemistry and Physics*, 19, 89–113, <https://doi.org/10.5194/acp-19-89-2019>, 2019.



470

Figure 1: Spatiotemporal variations in the concentrations of basic gases and other parameters during the Yellow and Bohai Sea cruise campaigns on December 9-22, 2019 (mapping TMA_{gas} by concentration (a); mapping onboard recorded wind speeds and directions (b); time-series of TMA_{gas} (c), DMA_{gas} , (d), $\text{NH}_{3\text{gas}}$ (e), and onboard recorded ambient air temperature (f); the time-series of SO_4^{2-} in $\text{PM}_{2.5}$ were shown as indicators of anthropogenic air pollutants in (d); not all data were shown in (b) to avoid clustering).

475

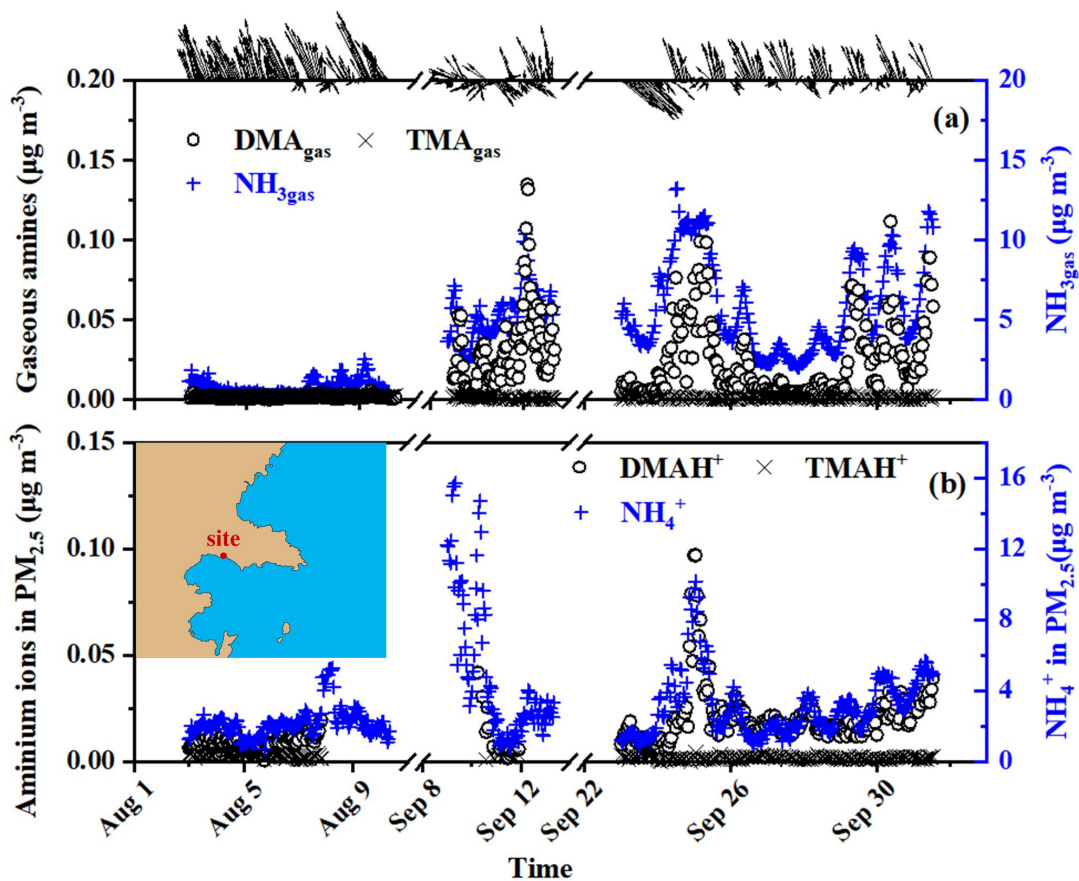


Figure 2: Temporal variations in the concentrations of $\text{NH}_{3\text{gas}}$ and gaseous amines and their counterparts in $\text{PM}_{2.5}$ at a coastal site during August and September 2019 ($\text{NH}_{3\text{gas}}$ and gaseous amines (a); counterparts in $\text{PM}_{2.5}$ (b); wind speed and direction superimposed on the top of (a); a map of the sampling site superimposed in (b); the missing data regarding amminium ions in $\text{PM}_{2.5}$ were due to occasional K^+ contamination (b)).

480

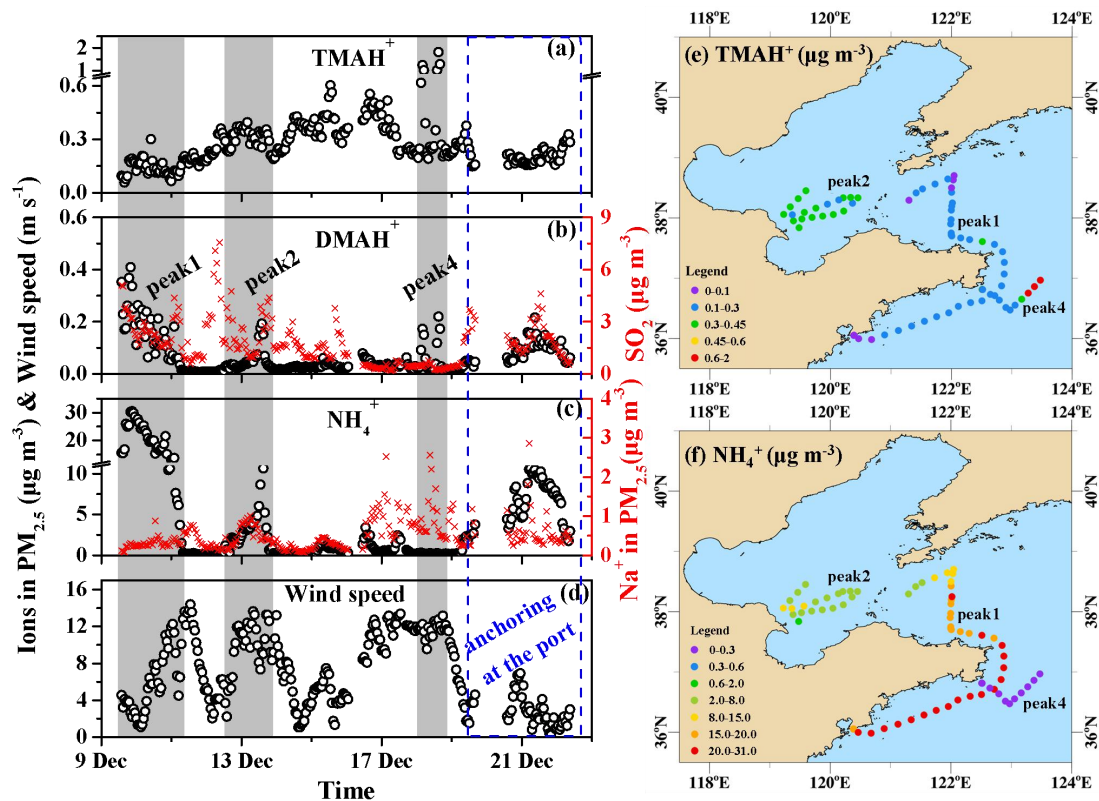


Figure 3: Spatiotemporal variations in the aminium ions and NH_4^+ concentrations of $\text{PM}_{2.5}$ and other parameters during the cruise campaign over the Yellow and Bohai Seas on 9-22 December 2019 (time-series of TMAH^+ (a), DMAH^+ (b), and NH_4^+ in $\text{PM}_{2.5}$ (c), wind speeds (WS) (d); mapping of the TMAH^+ in concentration (e); mapping of the NH_4^+ concentration (f); the time-series of SO_2 are shown as an indicator in (b); the time-series of Na^+ in $\text{PM}_{2.5}$ were shown as an indicator of sea spray aerosols in (c); only some data were used in (e) and (f) to avoid clustering)

485

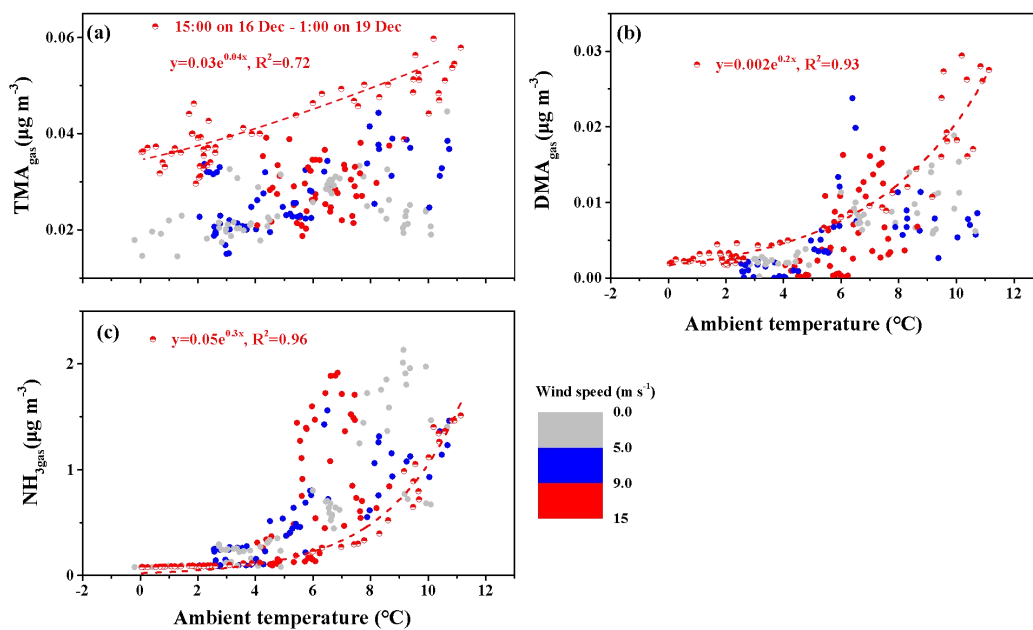


Figure 4: Correlations between the concentrations of basic gases and ambient temperature (TMA_{gas} (a); DMA_{gas} (b); and NH_3 (c); the colored bar represents different wind speeds; full symbols represent the data observed throughout the campaign excluding the period from 15:00 on December 16 to 01:00 on December 19).

490

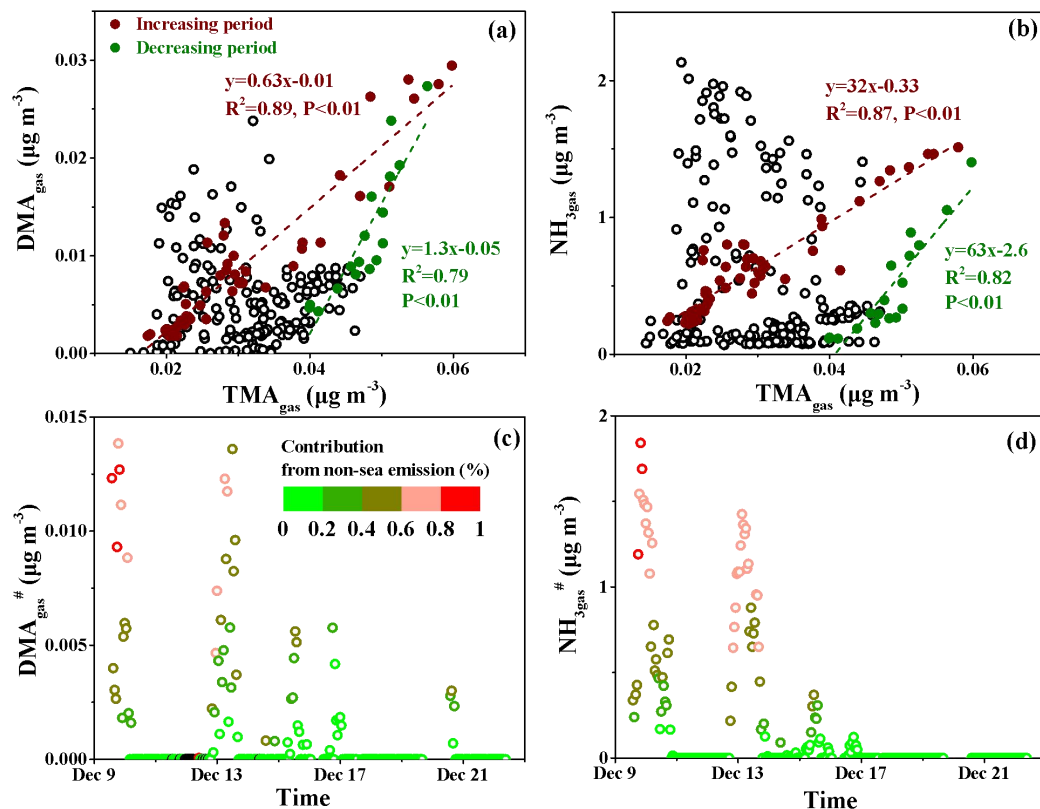
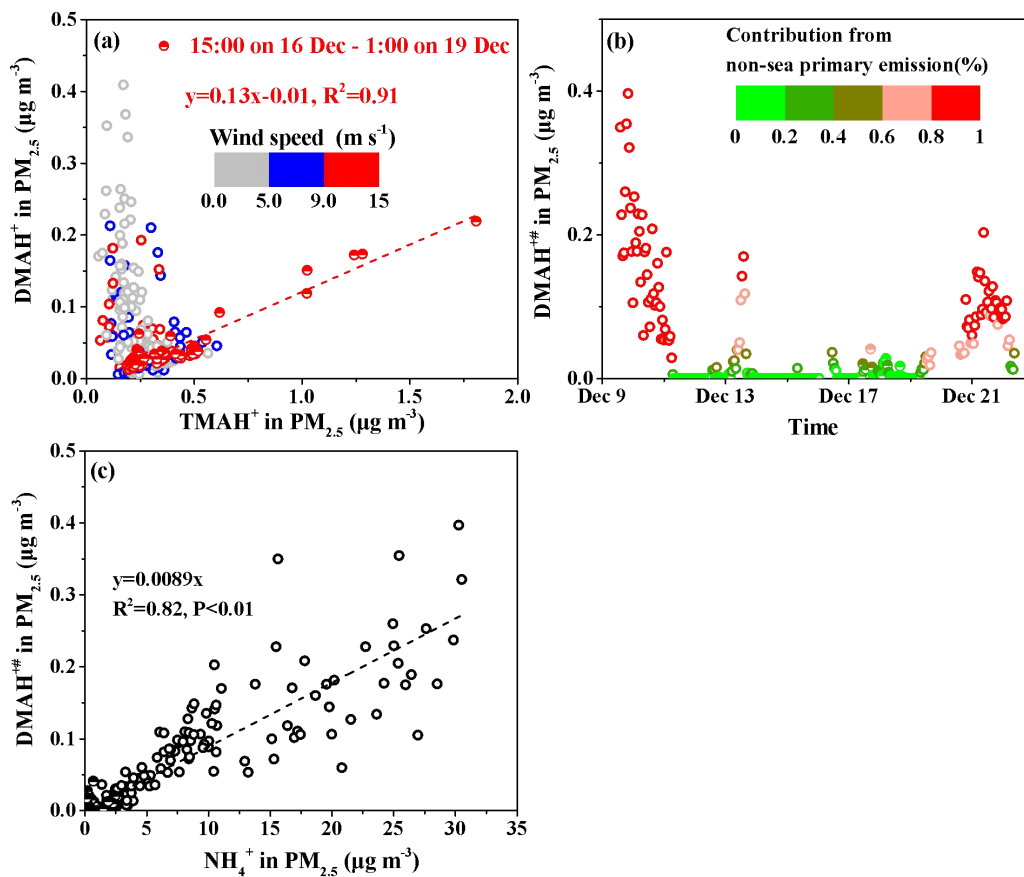


Figure 5: Correlations of DMA_{gas} and NH_{3gas} with TMA_{gas} and time-series of the calculated DMA_{gas}[#] and NH_{3gas}[#] (DMA_{gas} vs TMA_{gas} (a); NH_{3gas} vs TMA_{gas} (b); DMA_{gas}[#] (c); and NH_{3gas}[#] (d); the colored bars in (c) and (d) represent the percentages of transported DMA_{gas}[#] and NH_{3gas}[#] in each corresponding observed value).



495

Figure 6: Correlations analyses of different variables in PM_{2.5} and time-series of the calculated DMAH⁺ in PM_{2.5} (DMAH⁺ vs TMAH⁺ (a); time-series of DMAH⁺ (b); DMAH⁺ vs NH₄⁺; DMAH⁺ vs NH₄⁺).